Title
Probing Ionic Complexes of Ethylene and Acetylene with Vacuum-Ultraviolet Radiation.

Journal
The Journal of Physical Chemistry A, 120(27)

ISSN
1089-5639

Authors
Bandyopadhyay, Biswajit
Stein, Tamar
Fang, Yigang
et al.

Publication Date
2016-07-14

DOI
10.1021/acs.jpca.6b00107

Peer reviewed

J. Phys. Chem. A

Probing Ionic Complexes of Ethylene and Acetylene with Vacuum Ultraviolet Radiation

Biswajit Bandyopadhyay[1#], Tamar Stein[1,2#], Yigang Fang[1], Oleg Kostko[1], Alec White[1,2], Martin Head-Gordon[1,2]* and Musahid Ahmed[1]*

[1]Chemical Sciences Division, Lawrence Berkeley National Laboratory, 1 Cyclotron Road, Berkeley, California - 94720, United States

[2]Department of Chemistry, University of California Berkeley, Berkeley, California- 94720, United States

# Equal contributions

*M.H.-G.: E-mail: mhg@cchem.berkeley.edu, *M. A.: E-mail: MAhmed@lbl.gov.

ABSTRACT

Mixed complexes of acetylene-ethylene are studied using VUV photoionization mass spectrometry and theoretical calculations. These complexes are produced and ionized at different distances from the exit of a continuous nozzle followed by reflectron time-of-flight mass spectrometry detection. Acetylene, with a higher ionization energy (11.4 eV) than ethylene (10.6 eV), allows for tuning the VUV energy and initializing reactions either from a $C_2H_2^+$ or a $C_2H_4^+$ cation. Pure acetylene and ethylene expansions are separately carried out to compare and contrast, and hence identify products from the mixed expansion: these are $C_3H_3^+$ (m/z = 39), $C_4H_5^+$ (m/z = 53) and $C_5H_5^+$ (m/z = 65). Intensity distributions of C_2H_2, C_2H_4, their dimers and reactions products are plotted as a function of ionization distance. These distributions suggest that association mechanisms play a crucial role in product formation closer to the nozzle. Photoionization efficiency (PIE) curves of the mixed complexes demonstrate rising edges closer to both ethylene and acetylene IEs. We use density functional theory (ωB97X-V/aug-cc-pVTZ) to study the structures of the neutral and ionized dimers, calculate their adiabatic and vertical ionization energies, as well as the energetics of different isomers on the potential energy surface (PES). Upon ionization, vibrationally excited clusters can use the extra energy to access different isomers on the PES. At farther ionization distances from the nozzle, where the number densities are lower, unimolecular decay is expected to be the dominant mechanism. We discuss the possible decay pathways from the different isomers on the PES, and examine the ones which are energetically accessible.

INTRODUCTION

Mass spectrometry has been extensively used to characterize and identify clusters (and complexes) produced in molecular beams for the last few decades. Cluster intensity distributions, their formation and growth have been traditionally investigated by varying initial parameters such as temperature and pressure of the buffer gas.[1-2] Pulsed laser vaporization[3], electric discharge techniques[4] and electron impact ionization[5] etc. routinely produce complexes and clusters with different intensity distributions and internal temperatures when sampled from various regions of the supersonic expansion. Recently, Relph et al. have used an electron impact ionization source to produce acetylene and mixed acetylene-argon clusters where the timing between the pulsed ionization and the gas expansion was varied to sample different regimes of the expansion in which reactions either start from an acetylene cation or a neutral cluster.[5] We have previously used a continuous supersonic expansion to produce methanol clusters, and observed different ionization products and cluster growth mechanisms upon increasing the distance from the nozzle.[6]

Acetylene and its reaction products are key constituents in combustion and atmospheric processes.[7] Large acetylene clusters are predicted to play interesting roles in the atmospheres of different planets and their moons.[8] Acetylene is the smallest unsaturated hydrocarbon and its ion and radical fragments are likely to be a basic precursor to the formation of polycyclic aromatic hydrocarbons (PAHs).[9-10] Hence, there have been a number of mass spectrometry based experiments on acetylene over the last few decades. As early as 1968, Futrell and co-workers studies the ion-molecule reactions of acetylene and ethylene using a high pressure tandem mass spectrometer.[11-12] Acetylene clusters were investigated by photoionization techniques and the appearance energies of several dissociation channels were also reported.[13] Different buffer gases,

for example, helium and argon were used in later studies to produce both acetylene and mixed argon-acetylene clusters.[14-15] Washida and Sato also reported a photoionization mass spectrometric study of ethylene intracluster reactions focusing on different fragmentation channels via excess energy dissipation.[14] Intermediate size acetylene clusters were produced in a supersonic expansion and probed by electron impact ionization by Coolbaugh et al. [16] Relph et al. used IR spectroscopy to study structures of $(acetylene)_n$ clusters where various regimes within a supersonic expansion were sampled.[5] Farnik et al. used electron ionization with variable electron energy to obtain the threshold ionization efficiency curves of acetylene and mixed acetylene-argon clusters.[17] The kinetics and mechanisms of fragmentation in mixed ethylene and acetylene systems were reported by Bowers and coworkers.[18] The reaction dynamics between acetylene cation and ethylene was studied using a threshold photoion photoelectron technique by Dutuit and coworkers with an eye on probing the potential energy surfaces of this reaction at various collision energies.[19]

Theoretically, ethylene and acetylene clusters and reaction products have been investigated over the years, the focus being on characterizing the cyclobutadiene cation.[20-22] Hrouda et al. performed a detailed study on the $C_4H_4^+$ potential energy surface (PES), using CCSD(T)/cc-pVTZ and density functional theory (DFT) (B3LYP/6-31G*) levels of theory. They studied the possible stable isomers formed by reaction of acetylene with its ion, and the transition-states connecting the stable isomers.[23-24] In a recent study, Momoh et al.[25] used ion mobility experiments combined with theoretical modeling in order to explore the structures of the acetylene dimer cation. They employed DFT (at the PBE/aug-cc-pvdz level) to determine the lowest energy isomers of $C_4H_4^+$ and concluded cyclobutadiene cations were predominant. These are in agreement with the study

of Relph et al.[5] who reported vibrational predissociation spectra of cationic acetylene clusters confirming the cyclobutadiene cation structure.

The dimer cation resulting from a reaction of ethylene with its cation, particularly the cyclobutane isomer has been studied in depth.[22, 26-27] Jungwirth et al.[22] using QCISD(T)/6-31G* and UMP2/6-31G* levels of theory found a stable π-complex to be the primary product of this reaction, and studied rearrangement of this complex to form other products on the PES. Wiest [26] used DFT (B3LYP/6-311+G** level) to study the cyclo-conversion reaction of cyclobutane radical cation into a complex of ethylene and ethylene cation and suggested that the reaction takes place via a concerted mechanism. Recently, Bera et al.[28] studied the association mechanism of acetylene and ethylene with their cations as well as the mixed dimer cation using CCSD(T)/cc-pVTZ level of theory. They focused on the encounter complexes and found that in all cases, a four membered ring is the most stable structure without rearrangement. They also found less stable encounter complexes: a linear connectivity isomer and a bridge structure.

Guided by these previous experimental and theoretical work, we present a comprehensive study of pure and mixed complexes of C_2H_2/C_2H_4 focusing on reaction products based upon tunable photoionization energy and variable nozzle to ionization distance.

EXPERIMENTAL SECTION

The experiments were carried out in a continuous supersonic expansion cluster machine coupled to a three meter VUV monochromator on the Chemical Dynamics Beamline (9.0.2), located at the Advanced Light Source, Berkeley, California. The experimental set up has been described previously in detail.[6] Here, three different gas mixtures were prepared using a baratron pressure gauge: 5% C_2H_2 in 95% argon, 5% C_2H_4 in 95% argon and 5% each of C_2H_2 and C_2H_4 in

90% argon. We use the notation of 5% C_2H_2 and C_2H_4 as "pure" and 5% (C_2H_2 + C_2H_4) as "mixed" expansion throughout this paper. 400 Torr of these gas mixtures were expanded through a 100 μm nozzle to a differentially pumped chamber kept at a pressure of 2×10^{-4} Torr. The beam was intersected with the VUV radiation at various axial distances from the nozzle (2-25 mm) and the resulting ions are sampled into a reflectron time-of-flight mass spectrometer. The ionization distance was varied by changing the nozzle position with respect to the point of intersection of molecular and VUV beams. A set of four electrodes were used to guide the ions from the ionization region to the mass spectrometer through a skimmer. The lenses were kept at small potentials (+5, 0, -3, and 0 V, respectively) and the skimmer was grounded.

The mass spectrometer was kept at 2×10^{-6} Torr in the second differentially pumped chamber. A start pulse for the TOF was provided by pulsing both the repeller and accelerator plates because of the quasi-continuous (500 MHz) nature of the synchrotron light and investigation of the charged species. The ions were pulse-extracted by a fast switching of repeller and accelerator plates to 1100 and 1080V correspondingly. Ions were accelerated perpendicularly to their initial flight path through the field free region and detected by a microchannel plate (MCP) detector installed at the end of the tube. The mass spectrometer settings were kept fixed while the ionization distance was varied. The time dependent electrical signal from the detector was amplified by a fast preamplifier, collected by a multichannel scalar card, and then integrated with a computer. TOF spectra were measured at different positions in the photon energy range between 10 and 12 eV. The photoionization efficiency (PIE) curves were obtained by integrating peak intensities at each photon energy and normalized by the photon flux.

THEORETICAL SECTION

All calculations reported in this manuscript were carried out using Q-Chem 4.3.[29] The structures and relative energies were all calculated using density functional theory (DFT) using the ωB97X-V functional[30] with the aug-cc-pVTZ basis set. Geometry optimizations were followed by frequency calculations to verify that the optimized structures are local minima.

In order to obtain the transition-state structures, we use the freezing string method,[31] which applies the reactant and the product structures of the relevant reactions as input and uses them to construct guesses for the transition-state structures. These are further refined using local optimization to obtain the transition states. We performed frequency calculations to confirm that the structures are first-order saddle points.

ωB97X-V is a range-separated hybrid functional including non-local correlation which is designed to treat non-covalent interactions and as such is suitable for the description of the neutral hydrocarbon clusters studied in this manuscript. Moreover, as a range-separated functional, we can expect reduced self-interaction error,[32-33] meaning that the functional should be adequate for the description of radical cation clusters.[34]

RESULTS AND DISCUSSION

A. EXPERIMENTAL

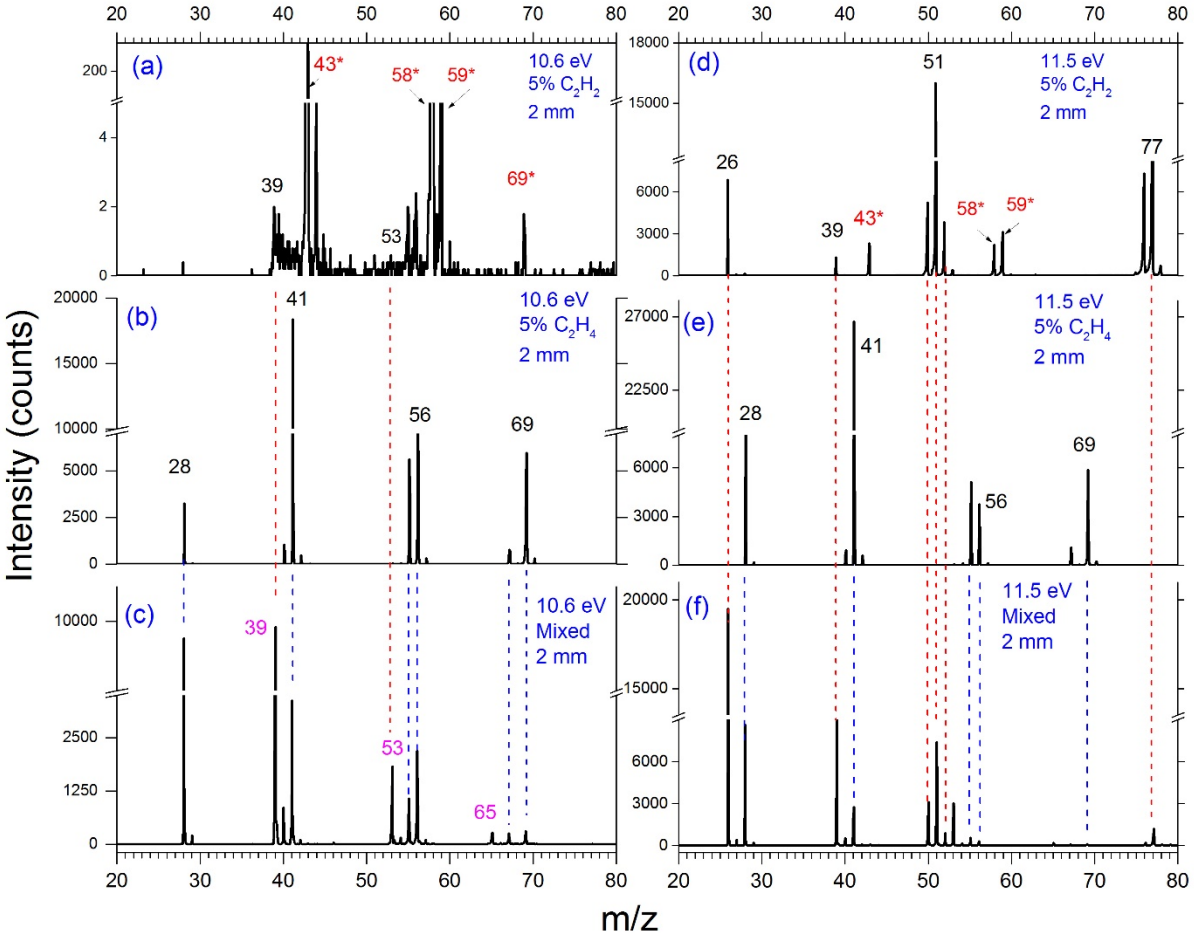

Figure 1. Mass spectra measured at (a, b, c) 10.6 and (d, e, f) 11.5 eVs when the ionization is carried out 2 mm downstream from the nozzle for (a, b, d, e) pure and mixed (c, f) C_2H_2/C_2H_4 expansions. C_2H_2 expansion shows some impurities from acetone (m/z = 43, 58, 59 and 69, marked as red stars). The peaks observed in C_2H_2 and C_2H_4 expansions are correlated to the mixed expansion by red and blue dashed lines, respectively. Three new peaks are prominent in the mixed expansion at 10.6 eV (c): m/z = 39, 53 and 65. At 11.5 eV, the peaks observed in the mixed expansions can be identified from the respective pure expansions (d, e, f).

Ionization energies (IE) of C_2H_4 and C_2H_2 are 10.5 and 11.4 eV, respectively.[35] Figure 1 shows representative mass spectra from C_2H_2, C_2H_4 and mixed expansions at an ionization distance of 2 mm using photon energies just above the respective IEs. At 10.6 eV, the C_2H_4 expansion shows five intense peaks (Fig. 1b): m/z = 28 ($C_2H_4^+$), 41 ($C_3H_5^+$), 55 ($C_4H_7^+$), 56 ($C_4H_8^+$) and 69 ($C_5H_9^+$). For the mixed expansion, three new peaks are observed (Fig. 1c): m/z = 39 ($C_3H_3^+$), 53 ($C_4H_5^+$) and 65 ($C_5H_5^+$). Few counts of m/z= 39 and 53 are seen in the acetylene expansion and mass 26 ($C_2H_2^+$) is not observed (Fig. 1a). The spectrum consists of peaks from acetone impurities (m/z = 43, 44, 58, 59 and 69, marked as red stars) identified via photoionization efficiency curves (see SI Figure S1). At 11.5 eV, above the IE of C_2H_2, the mass spectrum consists of seven main peaks (Fig. 1d): m/z = 26 ($C_2H_2^+$), 39 ($C_3H_3^+$), 51 ($C_4H_3^+$), 52 ($C_4H_4^+$), 76 ($C_6H_4^+$), 77 ($C_6H_5^+$) and 78 ($C_6H_6^+$). For the ethylene expansion at 11.5 eV (Fig. 1e), overall intensities of larger complexes decrease whereas those of monomer (m/z = 28) and $C_3H_5^+$ (m/z = 41) increase compared to 10.6 eV (Fig. 1b). The peaks observed for pure ethylene and acetylene expansions match the results from Washida et al.[14] However, we have not observed sizes larger than the trimer, probably because we used relatively low backing pressure (400 Torr compared to 760-1000 Torr of Washida et al.). The mixed expansion consists of peaks observed in individual expansions at 11.5 eV because both ethylene and acetylene moieties are ionized.

Figure 2 depicts mass spectra from pure and mixed expansions at farther ionization distance from nozzle, 20 mm, using the same VUV energies. For pure expansions, comparing Fig. 1b (C_2H_4 expansion, 10.6 eV, 2 mm) to Fig. 2a (C_2H_4 expansion, 10.6 eV, 20 mm) and Fig 1d (C_2H_2 expansion, 11.5 eV, 2 mm) to Fig. 2c (C_2H_2 expansion, 11.5 eV, 20 mm) it is clear that the

intensities of monomers are significantly higher at 20 mm distance compared to those at 2 mm. On the other hand, larger complexes (m/z = 41, 55, 56, 67 and 69 for the C_2H_4 expansion (compare Fig. 1b to 2a) and m/z = 50, 51, 52, 76, 77, 78 for C_2H_2) are weaker (compare Fig. 1d to 2c). For mixed expansions, both at 10.6 and 11.5 eV, we observe relatively lower amounts of masses 39 and 53 compared to those at 2 mm and m/z = 65 is not observed (compare Fig. 1c [mixed, 10.6 eV, 2 mm] to Fig. 2b [mixed, 10.6 eV, 20 mm, and Fig. 1f [mixed, 11.5 eV, 2 mm] to Fig. 2d [mixed, 11.5 eV, 20 mm]).

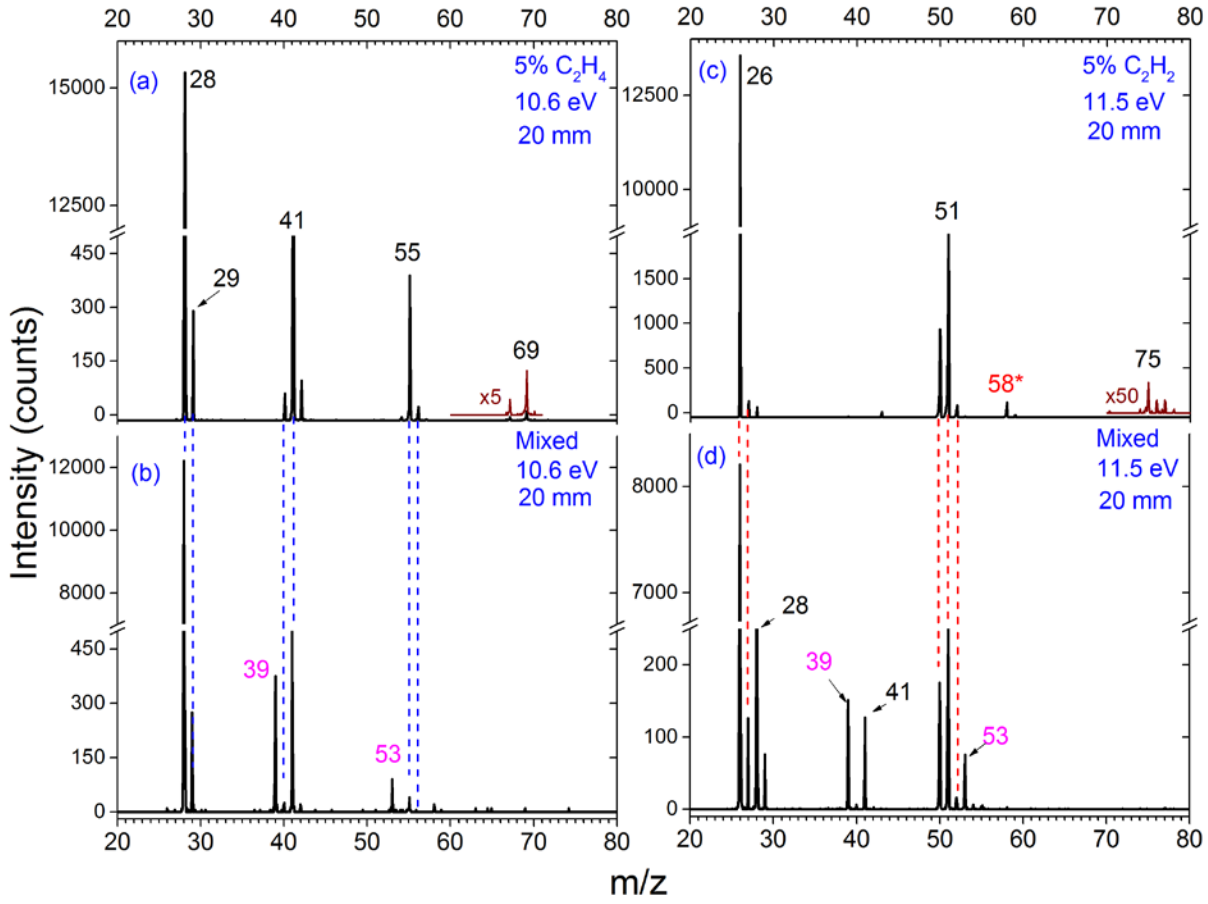

Figure 2. Mass spectra measured for C_2H_4 and mixed C_2H_4 / C_2H_2 expansions at (a, b) 10.6 eV at 20 mm ionization distance. Panels (c) and (d) show spectra for C_2H_2 and mixed expansions at 11.5 eV. The intensities of monomers are greater than those at closer distance, whereas cluster abundances are comparatively low. Blue and red dashed lines are used to correlate the peaks from mixed to pure expansions.

The characterization of supersonic expansions from a small nozzle has been extensively studied in the last few decades.[1-2] It is well established that maximum collisions occur at the nozzle-exit, and both number densities and temperature drastically decreases within a very few

nozzle diameters along the beam propagating axis. Therefore, it is expected that the neutral cluster formation ceases within a few mm from the exit. Precisely controlled monochromatic VUV photons allow for soft ionization without imparting extra internal energy to the monomer. However, ionization of a cluster can lead to charge redistribution and/or post ionization reactions. Without any post ionization dynamics, sampling from different regimes of the expansion, the intensity distribution of a species (both monomer and clusters) is expected to follow the similar trend defined by the number density along the beam propagating axis. On the other hand, intensities should deviate from the regular distributions if post ionization dynamics dominate. These dynamics are observed in our previous publication, where mass spectra showed interesting distributions of protonated methanol clusters as a function of ionization distance using the same experimental set up.[6] Post ionization association reactions can start from the reaction of a monomer ion (M) with neutral (N) for example,

$$M^+ + N \rightarrow MN^+ \quad (1)$$

or an ion produced from a higher cluster (C_n),

$$C_n^+ \rightarrow C_{n-1}^+ + C \quad (2)$$

where C_{n-1}^+ reacts with another neutral species.

At closer ionization distances where the number densities are higher, there is a higher probability of M^+ or C_{n-1}^+ finding another neutral moiety (can be either monomer or a cluster, C_n). We will elaborate on the above assumptions using the intensity distributions of acetylene monomer, dimer ($C_4H_4^+$) and a reaction product ($C_4H_3^+$).

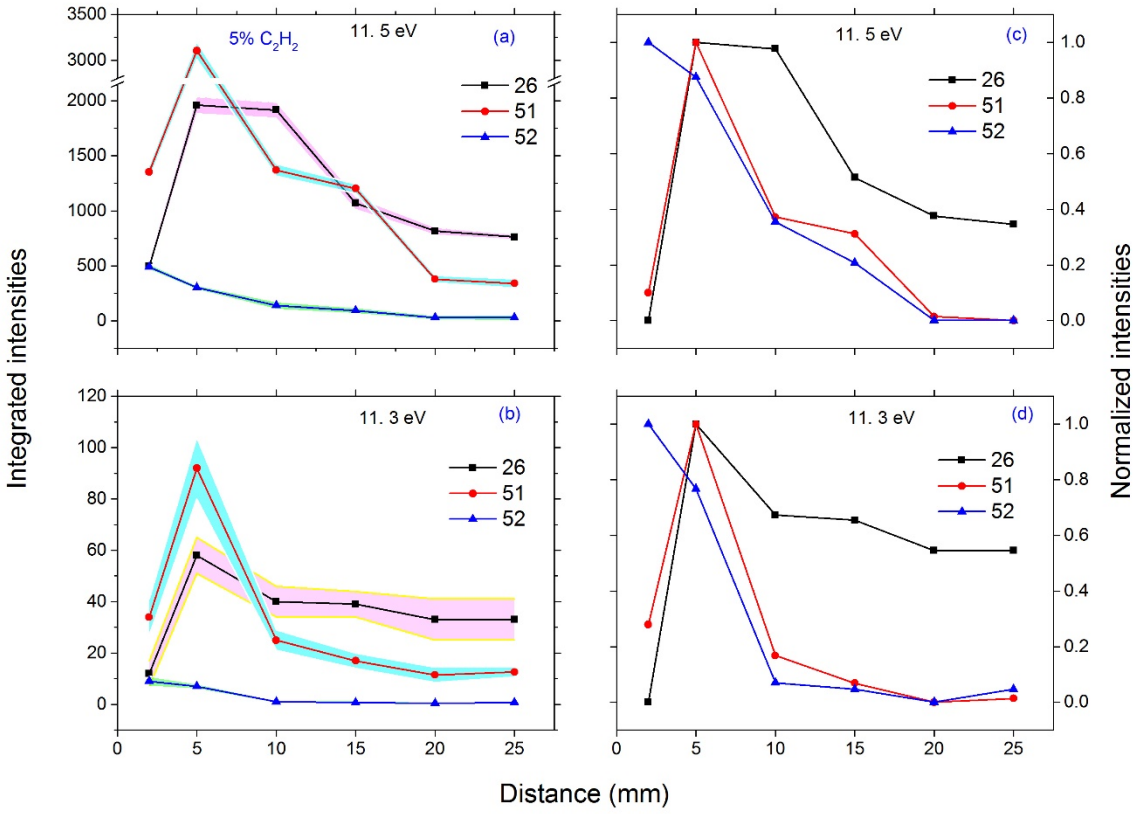

Figure 3. Integrated intensities of m/z = 26 ($C_2H_2^+$), 51 ($C_4H_3^+$) and 52 ($C_4H_4^+$) from C_2H_2 expansion at (a) 11.5 eV and (b) 11.3 eV photon energies as a function of distance from nozzle to ionization. The experimental uncertainties are shown as colored shades for each ion. Normalized intensities for the same ions are shown in panels (c) and (d) for 11.5 and 11.3 eV, respectively. Intensities are significantly less below the IE of C_2H_2. While m/z = 26 and 52 show maxima at 5 mm, the distribution of m/z = 52 gradually decreases with distance. The trend of these distributions can be clearly seen in normalized intensity plots (panel c and d).

Figure 3 shows the integrated intensities of m/z = 26 ($C_2H_2^+$), 51($C_4H_3^+$) and 52 ($C_4H_4^+$) from an acetylene expansion. The top (a, c) and bottom traces (b, d) depict the distributions above (11.5 eV) and below (11.3 eV) the IE of acetylene. We note that the ion intensities of $C_2H_2^+$, $C_4H_3^+$ and $C_4H_4^+$ at 11.3 eV are significantly less in magnitude than those at 11.5 eV (compare ~ 60-40, 100-20 and 15-5 at 5 mm at 11.3 eV to ~2000-500, 3000-1000 and 500-50 at 2-25 mm range at 11.5 eV of integrated intensities for m/z = 26, 51 and 52). Above the IE of C_2H_2, $C_2H_2^+$ is formed which subsequently reacts with a free C_2H_2 (or $(C_2H_2)_n$ clusters) to form $C_4H_4^+$ and $C_4H_3^+$ ions.

$$C_2H_2 + h\nu \rightarrow C_2H_2^+ + e^- \quad (3)$$

$$C_2H_2^+ + C_2H_2 \rightarrow C_4H_4^+ \rightarrow C_4H_3^+ + H \quad (4)$$

$$C_2H_2^+ + C_2H_2 \rightarrow C_4H_2^+ + H_2 \quad (5)$$

At this energy, neutral acetylene clusters can also be ionized, which can undergo elimination reactions to form m/z = 26, 51 and 52.

$$(C_2H_2)_2 + h\nu \rightarrow (C_2H_2)_2^{+*} + e^- \rightarrow C_4H_3^+ + H + e^- \quad (6)$$

$$(C_2H_2)_2^+ \rightarrow C_2H_2^+ + C_2H_2 \quad (7)$$

$$(C_2H_2)_3^+ \rightarrow C_4H_4^+ + C_2H_2 \quad (8)$$

$$(C_2H_2)_3^+ \rightarrow C_4H_3^+ + C_2H_2 + H \quad (9)$$

The density of monomer (C_2H_2) is expected to be maximum closer to the exit and it gradually diminishes as expansion proceeds farther following the distributions described in references 1-2. At any given distance, we know that usually cluster densities are less than the

monomer. For example, above the IE of methanol in a methanol-argon expansion, CH_3OH^+ is the dominating peak in the mass spectrum, and its protonated counterpart is less intense.[36] Similarly, H_2O^+ cation dominates the mass spectrum in a water-argon expansion at 12.6 eV (IE of water).[37] Therefore, above the IE of acetylene, formation of $C_2H_2^+$ and its subsequent reactions (eqns. 3-5), as well as fragmentations of larger clusters (eqns. 6-9) produces the ions in Fig. 3.

Below the IE of acetylene (11.3 eV), the C_2H_2 monomer is not ionized and therefore $C_2H_2^+$ can only form from larger clusters because these can be ionized at lower energies due to solvation. Similar observation was made for methanol and water clusters where solvation leads to lowering of IEs. Therefore, the counts observed in Figure 3b and 3d are mostly from fragmentations of the larger clusters (eqns. 6-9). The intensities of ions at this energy is significantly less because - a) C_2H_2 monomer is not ionized and b) ionization efficiency of clusters are less at lower energies. However, we cannot rule out the possibility that at 11.3 eV, $C_2H_2^+$ formed from a larger cluster undergoes reactions 4 and 5 with a lesser efficiency. Reactions 4 and 5 starting from a $C_2H_2^+$ which forms from a higher cluster would have a higher probability of occurring at closer distances as postulated in eqn. 2. It is also possible that $C_2H_2^+$ can undergo reactions within a cluster (i.e., intracluster) to form the observed ions in Figure 3. For example, eqn. 6 is another way of writing eqn. 4 for the intracluster case. However, the probability of intracluster reactions is a function of the cluster population itself and hence it should follow the diminishing trend as a function of distance. Below the IE of acetylene, the extent of cluster fragmentation, as well as intracluster reactions are expected to be less which leads to fewer ion intensities (Fig. 3b) than at 11.5 eV (Fig. 3a). Here, it is important to mention that to explain the intensity distributions in Figure 3, even though we have written fragmentations from up to the trimer as equations, larger cluster

fragmentation can also occur. Again, it should be noted that larger cluster fragmentation would be a function of neutral cluster population with distance.

We also notice that for both photon energies above and below the IE of acetylene, m/z = 52 ($C_4H_4^+$) shows maximum intensity at 2 mm followed by a gradual decrease with distance. On the other hand, the intensities of m/z = 26 ($C_2H_2^+$) and 51 ($C_4H_3^+$) go through maxima at an intermediate distance (5 mm). To show the distribution trends more clearly, we plot the normalized intensities in Fig. 3c and 3d. The intensity of $C_2H_2^+$ is less at 2 mm than that of 5 mm because closer to the nozzle, reactions 4 and 5 form $C_4H_3^+$ and $C_4H_2^+$. It is mentioned above that $C_2H_2^+$ forms from both direct ionization and from larger clusters at 11.5 eV, and in both cases, the probability of ion-molecule reactions is higher at closer ionization distance leaving less $C_2H_2^+$ and producing more $C_4H_3^+$ (and $C_4H_2^+$). Following this logic, we see more $C_4H_3^+$ than $C_2H_2^+$ at 2 mm. From 5-20 mm, since the ion-molecule reactions are less and only intracluster and larger cluster fragmentations are dominating, ion-intensity distribution follow the gradual diminishing density trend for both $C_2H_2^+$ and $C_4H_3^+$. The intensities of these ions are maximum at 5 mm because at this distance, both ion-molecule and larger cluster fragmentations give rise to observed intensities of ions. The dimer ($C_4H_4^+$) shows a diminishing distribution as a function of ionization distance indicating that it mostly forms from larger clusters. Similar trend of these ion distributions are observed at 11.3 eV (below the IE of acetylene) since $C_2H_2^+$ formed from larger clusters undergoes reactions 4 and 5 (ion-molecule) and probably a small amount of intracluster reactions with less efficiency.

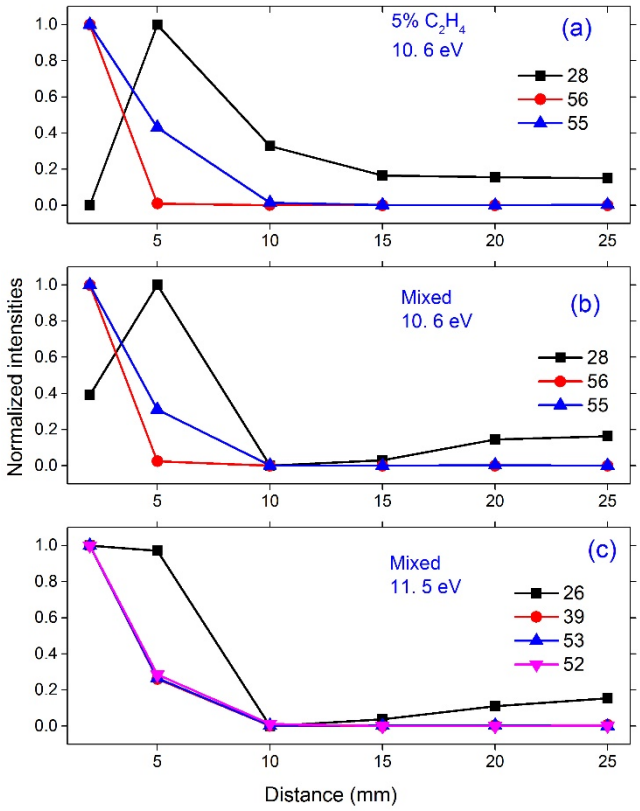

Figure 4. Normalized intensities of various fragments measured at 10.6 (a, b) and 11.5 eV (c) photon energies as a function of distance for pure ethylene (a) and mixed (b, d) expansions. For the C_2H_4 expansion, monomers (m/z = 26) shows maximum intensity at 5 mm. For the mixed expansion, the intensities of monomers show a slight increase after a minimum at 10 mm. Reaction products of the mixed expansion m/z= 39 and 53 follow the diminishing distribution trend.

Having described the intensity patterns for the C_2H_2 expansion, we can now discuss distributions for C_2H_4 and mixed expansions. Figure 4 displays normalized intensities of m/z = 28 ($C_2H_4^+$), 56 ($C_4H_8^+$) and 55 ($C_4H_7^+$) for both C_2H_4 and mixed expansions at 10.6 eV (Fig. 4a and b). For both expansions at 10.6 eV, similar to the C_2H_2 distribution, the intensity of $C_2H_4^+$ (28)

shows a maximum at 5 mm. The intensity of mass 56 (the ethylene dimer cation) also shows a similar distribution as the acetylene dimer cation (m/z = 52). Here, in contrast to the acetylene reaction, the product of reaction (11), $C_4H_7^+$ (m/z = 55) shows the highest intensity at 2 mm. The trend observed in ethylene and mixed expansions at 10.6 eV again can be comprehended by the following reactions:

$$C_2H_4 + h\nu \rightarrow C_2H_4^+ + e^- \quad (10)$$

$$C_2H_4^+ + C_2H_4 \rightarrow C_4H_7^+ + H \quad (11)$$

$$C_2H_4^+ + C_2H_4 \rightarrow C_3H_5^+ + CH_3 \quad (12)$$

$$(C_2H_4)_2 + h\nu \rightarrow (C_2H_4)_2^+ \rightarrow C_2H_4^+ + C_2H_4 \quad (13)$$

$$(C_2H_4)_3 + h\nu \rightarrow (C_2H_4)_3^+ \rightarrow C_4H_8^+ + C_2H_4 \quad (14)$$

Reactions 11-12 represent ion-molecule reactions which should be prevalent above the IE of ethylene. At 10.6 eV, larger cluster fragmentation followed by ionization can produce ethylene monomer and dimer cations ($C_2H_4^+$ and $C_4H_8^+$) as depicted in reactions 13 and 14. We see very few counts of ions below the IE of ethylene (not shown here) which indicates that in this case intracluster reactions below the IE of ethylene are not dominant. Here, again, even though we are writing fragmentation from up to trimer, larger cluster fragmentations are also possible. The intensity of m/z = 28 shows a minimum at 2 mm for both ethylene and mixed expansions, similar to the acetylene monomer example described before, ion-molecule reactions of $C_2H_4^+$ depletes the overall monomer intensity at closer distances (eqns. 11 and 12). Again, $C_2H_4^+$ can form from direct ionization or cluster fragmentation, and irrespective of formation mechanisms, $C_2H_4^+$ has a better probability for ion-molecule reactions at closer distances. Masses 55 and 56 show the normal

density distributions where the intensity of m/z = 55 is higher than m/z = 56 at 5 mm, suggesting that the dimer is forming from the larger clusters and m/z = 55 from both ion-molecule and fragmentations from larger clusters. The intensity of m/z = 28 shows a slightly different behavior in the mixed expansion, where it displays a minimum at 10 mm followed by a gradual increase. The reactions from the mixed expansions are the following: ion-molecule reactions-

$$C_2H_4^+ + C_2H_2 \rightarrow C_3H_3^+ + CH_3 \quad (15)$$

$$C_2H_4^+ + C_2H_2 \rightarrow C_4H_5^+ + H \quad (16)$$

Or ionization of a mixed neutral complex followed by fragmentation:

$$(C_2H_4\text{-}\ C_2H_2)^{+}* \rightarrow C_3H_3^+ + CH_3 \quad (17)$$

$$(C_2H_4\text{-}\ C_2H_2)^{+}* \rightarrow C_4H_5^+ + H \quad (18)$$

Where the extra energy is carried out by neutral CH_3 or H.

The other possible reaction to form m/z = 39 ($C_3H_3^+$) is from dissociation of the acetylene trimer:

$$(C_2H_2)_3^+ \rightarrow C_3H_3^+ + C_3H_3 \quad (19)$$

Both m/z= 39 and 53 can also form by ion-molecule reactions of the acetylene cation ($C_2H_2^+$):

$$C_2H_2^+ + C_2H_4 \rightarrow C_3H_3^+ + CH_3 \quad (20)$$

$$C_2H_2^+ + C_2H_4 \rightarrow C_4H_5^+ + H \quad (21)$$

However, at 10.6 eV, which is below the IE of acetylene, we observe a few counts of m/z = 39 (Fig. 1a) in the C_2H_2 expansion, and about 10,000 counts at 2 mm (Fig. 1c) for the mixed expansion suggesting that m/z = 39 is forming from a mixed C_2H_2/ C_2H_4 reaction initiating from a $C_2H_4^+$ cation (eqn. 15) and ionization of the mixed complex (eqns. 17-18). We will describe the

possibility of reactions 17 and 18 in the theoretical section below. Similarly, m/z = 53 is also observed in the mixed expansion at 10.6 eV which is below the IE of acetylene. PIE curves for these fragments are then expected to provide some insight into the formation pathways. Figure S2 shows the PIE curves for m/z = 39 and 53 as a function of distance for a mixed expansion. For both of these species, there are two distinct sharp rises - one at 10.5 eV and another at 11.4 eV. These curves clearly suggest that these products are from reactions 15-16, which display a rise at 10.5 eV. On the other hand, another sharp rise around 11.4 eV shows evidence of reactions 20-21. We note that reactions 17-18 are also possible but we do not see much change in threshold ionization. The energy threshold of $C_3H_3^+$ from any $(C_2H_2)_n$ cluster (eqn. 19) is 13.7 eV.[17] On the other hand, threshold for $(C_2H_2)_n^+$ is 11.7 eV which indicates that $C_3H_3^+$ is a product of mixed reactions, rather than fragmentation from larger acetylene clusters.

B. THEORETICAL

To understand the formation mechanisms of various species observed in the experiment, we have used theoretical calculations. The hypothesis is that farther from the nozzle, densities are much lower and so number distribution would reflect the unimolecular fragmentation dynamics. Any deviation closer to the nozzle would then represent association dynamics. Therefore, first we look at the distributions of various peaks at an ionization distance of 20 mm (Fig. 2) guided by theoretical calculations.

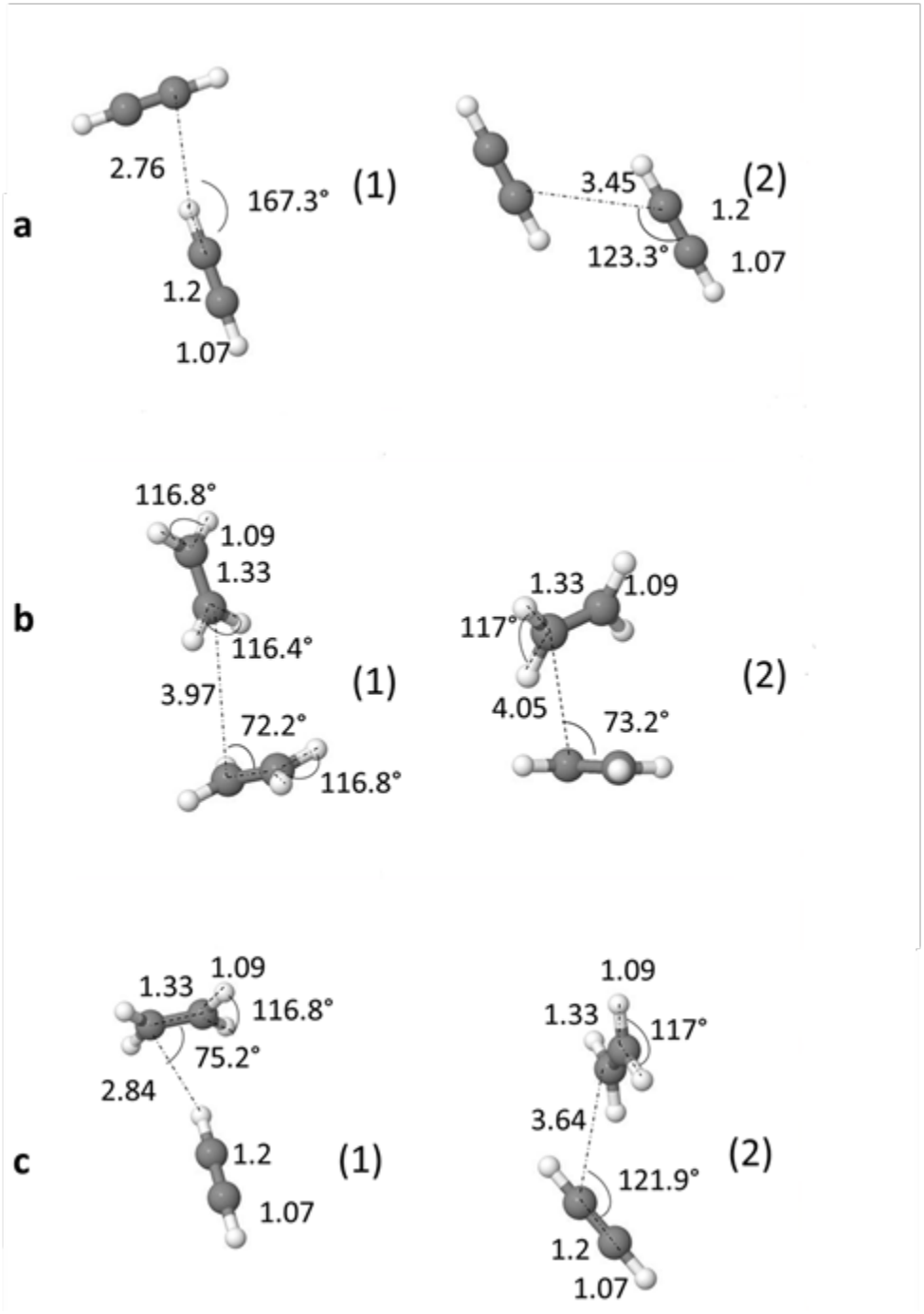

Figure 5: Neutral dimer structures of the different systems. (a) acetylene-acetylene dimer, (b) ethylene-ethylene dimer, and (c) mixed acetylene-ethylene dimer.

Figure 5 displays the neutral dimer clusters of the three systems discussed in this manuscript: the acetylene-acetylene dimer, the ethylene-ethylene dimer, and the mixed acetylene-ethylene dimers. For the acetylene dimer (Figure 5a), two local minima are a T-shaped and a slipped parallel structure. Both structures have been reported in the computational literature and experimentally observed.[38-40] These two structures are very close in energy: there is less than 0.2 kcal/mol difference between them, with the T-shaped structure being the lower one. In the T-shaped structure, the partially positively charged hydrogen is pointing toward the π electron cloud of the second acetylene while in the slipped parallel structure, the partially charged hydrogen is aligned with the partially negatively charged carbons.

The ethylene dimer structures are presented in Figure 5b. Again, the structures are very close in energy and are governed by CH-π interactions. The partially charged hydrogens point towards the π electron cloud of the second monomer. The distances between monomers are longer than for the acetylene dimers. Similar trends can be identified in the mixed structures. Here again there are two low energy structures, one which resembles the T-shaped and a second which resembles the slipped parallel one (Figure 5c).

Upon ionization, the no-longer-optimal neutral structures relax to more stable structures on the ionic surface. For the acetylene dimer, there are two resulting cation structures. A T-shaped isomer is obtained, with the distance between the two monomers decreased relative to the neutral structure; while the distance between the carbons and hydrogen is 2.76Å at the neutral structure, this distance is reduced to 2.16Å for the cation structure, as one would expect. The second structure is derived from the slipped parallel structure and is fully bonded. This structure was identified by Bera et al. as one of the stable structures of $C_4H_4^+$ and we will follow their notation and refer to it

as C2.[28] The C2 structure is shown in Figure 6.

All the different isomers of the neutral ethylene dimer also lead to a C2 cation structure, shown in Figure 7. For this structure the distance between the carbon atoms is calculated to be larger than in the acetylene case (2.09Å compared to 1.66Å for acetylene). Lastly, we examine the structure derived from re-optimization of acetylene-ethylene dimers. Here the resulting structure is a bridge one, following the notation of Bera et al. The bridge structure is shown in Figure 8. The structure is fully bonded with an inter-monomer carbon-carbon distance of 1.65Å.

Table 1 presents the adiabatic and vertical IE's for the monomers and their dimers. Vertical and adiabatic IE's are obtained by calculating the energy difference between the neutral and the ion structures. The vertical IE values were calculated as the energy difference between the neutral and the ion states where both are in the neutral optimal geometry. The adiabatic IE values were calculated as the energy difference between the neutral structures and the relaxed ion structures, i.e. in the ion optimal structures. The vertical IE's for the monomers are 11.32 eV for acetylene and 10.52 eV for ethylene. These values are in excellent agreement with the values reported in the literature which are 11.4 eV for acetylene and 10.5 eV for ethylene.[35] Table 1 also shows the IE's of the different dimer structures, as one can see from the table the IE's of the dimers are lower than those of the monomers.

In order to estimate the excess energy of the different structures which gives rise to decomposition and fragmentation of the complexes upon ionization, we will compare the vertical IE to the adiabatic IE as given in Table 1. For the acetylene dimers, we see that for the T-shaped structure, the difference between adiabatic and vertical IEs is only 0.22 eV, while the difference between the adiabatic and vertical IE's for the slipped parallel structure is much larger: 1.48 eV.

Significant differences, ranging between 1.29 eV and 1.44 eV, are also observed for the ethylene clusters. However, the biggest difference between the adiabatic and vertical IE is observed for the mixed dimers: 2.03 eV for the first isomer and 1.78 eV for the second one.

The excess internal energy means that the cations are vibrationally excited. At farther distances from the nozzle, where the number densities are low, vibrational relaxation are unlikely to be achieved by collisions with argon atoms or other clusters. Instead, the excess energy is sufficient to fragment the molecule (i.e. unimolecular decomposition), giving products with reduced internal energy. Below, we will discuss the stable isomers on the potential energy surfaces that are accessible in the experiment conditions, and the different available fragmentation pathways.

Table 1. Vertical and adiabatic ionization energies of acetylene and ethylene monomer and dimers. Isomer labels in parentheses match the neutrals shown in Fig. 5 and in SI (Fig. S3). The ionized species are depicted in Fig. 6, 7 & 8. The vertical and adiabatic IE's are calculated through the energy difference between the neutral and the ion at the relevant geometry.

Structure (isomer)	**Vertical IE (eV)**	**Adiabatic IE (eV)**
C_2H_2	11.31	11.19
C_2H_4	10.52	10.31
$(C_2H_2)_2$ (1)	11.00	10.78
$(C_2H_2)_2$ (2)	10.94	9.46
$(C_2H_4)_2$ (1)	10.36	8.97
$(C_2H_4)_2$ (2)	10.28	8.99
$(C_2H_4)_2$ (3)	10.45	9.00
$(C_2H_4)_2$ (4)	10.45	9.00
$(C_2H_4)_2$ (5)	10.34	8.99
$(C_2H_2•C_2H_4)$ (1)	10.67	8.64
$(C_2H_2•C_2H_4)$ (2)	10.41	8.63

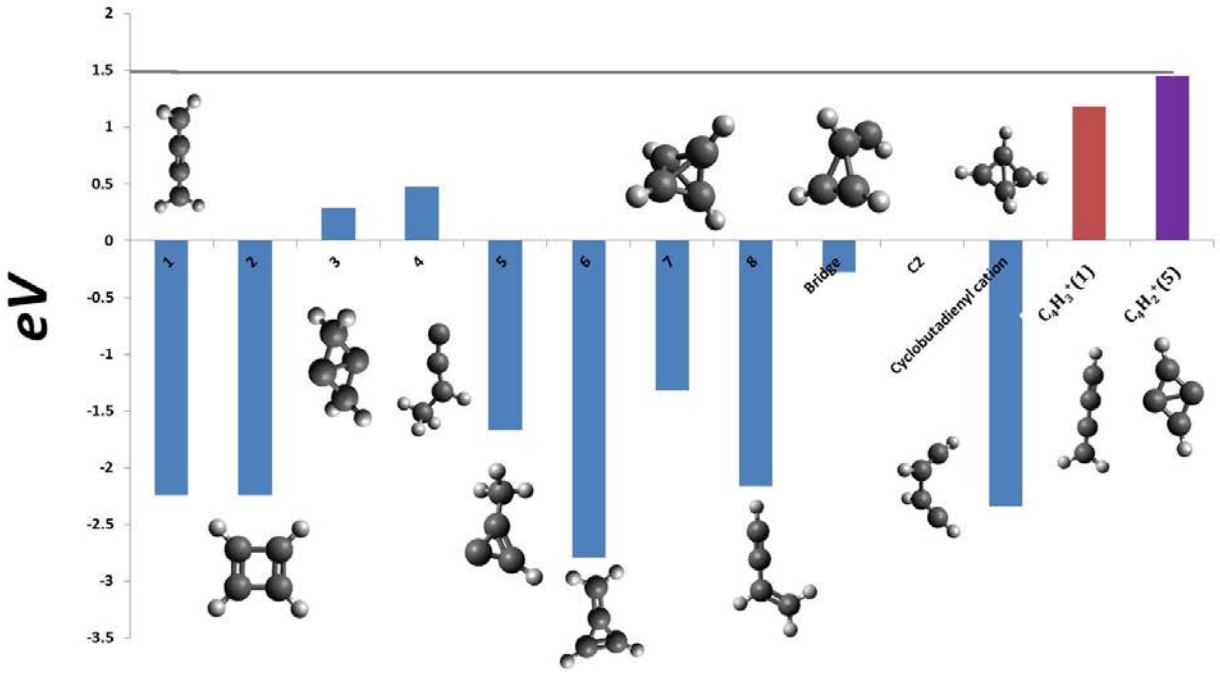

Figure 6. Relative energies of the different $C_4H_4^+$ isomers with respect to the cation optimized C2 structure. In blue are the relative energies of $C_4H_4^+$ isomers. In red is the relative energy of $C_4H_3^+$ + H. In purple is the relative energy of $C_4H_2^+$ + H_2. Numbers in parentheses refer to isomer labels (see Supplementary Materials). The light gray line at 1.48 eV indicates the total energy based on vertical ionization of neutral $(C_2H_2)_2$.

Figure 6 shows the energies of different isomers on the $C_4H_4^+$ potential energy surface, relative to the C2 structure. Without rearrangement (i.e. hydrogen migration) the stable structures are the C2, bridge and cyclobutadienyl cation. The relative energies are with respect to the C2 structure that is obtained upon relaxation of the ionized complex in the experiment (which itself is

formed with 1.48 eV of internal energy based on the IE differences of the slipped parallel structure). The bridge structure is very close in energy to the C2 structure with a very small barrier between the two[28], and with the available excess energy, crossing this barrier will be rapid. The most stable structures are found to be three and four membered ring structures. The three membered ring structure, isomer number 6 in Figure 6, is the lowest in energy; it derives stability from partial localization of positive charge on the tertiary carbon. This structure can be obtained from the bridge structure via hydrogen migration, with a barrier of 0.93 eV which is certainly accessible under the conditions of the experiment. The next most stable structure is cylobutadiene, which is also readily formed. We found two such structures, the puckered one found by Bera et al. and an additional linear isomer, which is slightly lower in energy (0.07 eV lower) by our DFT calculations.

The fragmentation pathways of the $C_4H_4^+$ ion include fragmentation by hydrogen loss to form $C_4H_3^+$ and loss of H_2 to form $C_4H_2^+$. As one can see from Figure 2, the intensity of $C_4H_3^+$ (m/z = 51) is higher than $C_4H_2^+$ (m/z = 50). This is because the loss of H_2 probably requires a concerted mechanism. Some more insight can be obtained by examining the optimal structure of $C_4H_3^+$ and $C_4H_2^+$. Figure 6 also shows the relative energies of $C_4H_3^+$ + H (red) and $C_4H_2^+$ + H_2 (purple) isomers which are energetically accessible under the experimental conditions. All the stable structures can be found in Supporting Information, SI (Figures S4 and S5). Among the $C_4H_3^+$ isomers, only one is energetically accessible. The accessible isomer is obtained from $C_4H_4^+$ isomers 1 or 8 by hydrogen loss. Among $C_4H_2^+$ isomers, although isomer 5 is accessible, it is much higher in energy and approaching the available energy of the system. This isomer likely results from fragmentation of $C_4H_4^+$ isomer number 7.

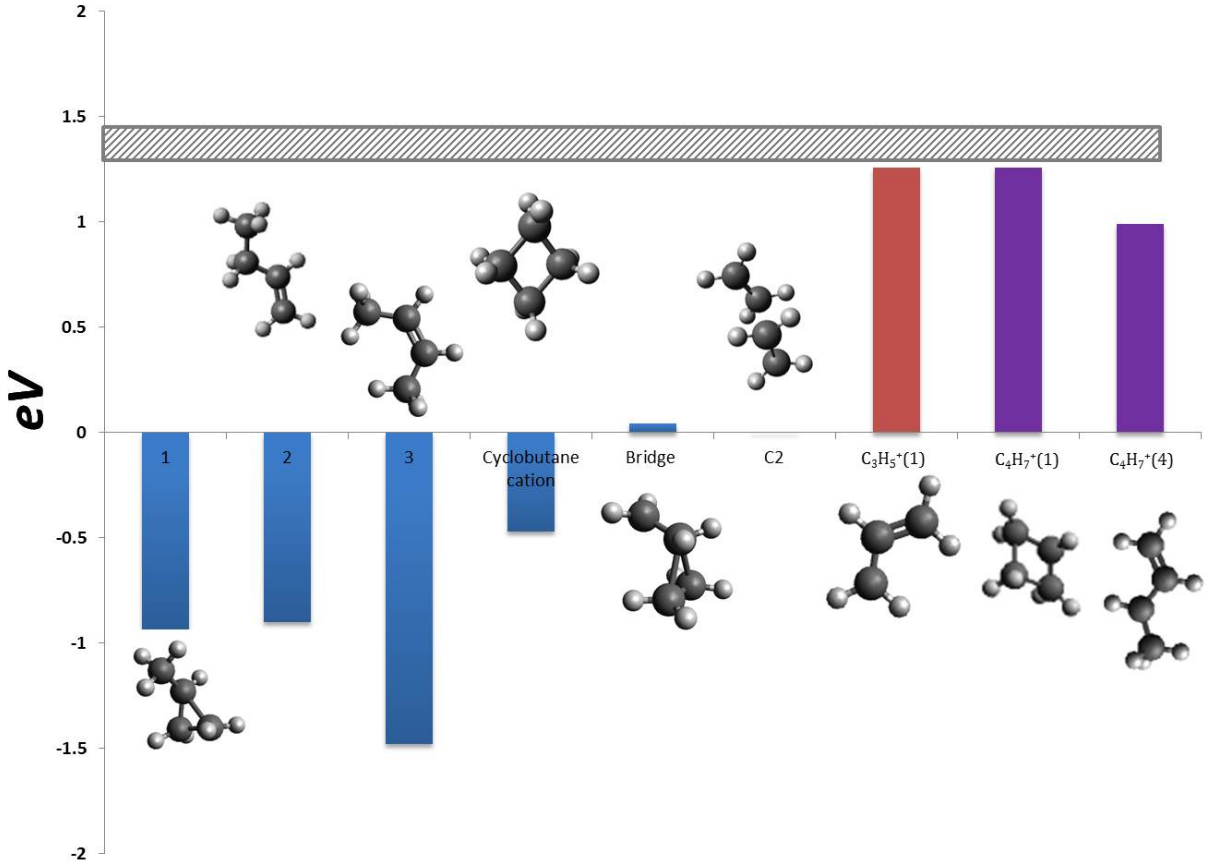

Figure 7. Relative energies of the different $C_4H_8^+$ isomers with respect to the cation optimized C2 structure. In blue are the relative energies of $C_4H_8^+$ isomers. In red is the relative energy of $C_3H_5^+$ + CH_3. In purple is the relative energy of $C_4H_7^+$ + H. Numbers in parentheses refer to isomer labels (see SI). The light gray band from 1.29 eV to 1.44 eV indicates the range of total energies based on vertical ionization of neutral $(C_2H_4)_2$.

Figure 7 shows the stable isomers of $C_4H_8^+$ with respect to the C2 isomer. The C2 and bridge isomers are very close in energy with the cyclobutane cation being the most stable isomer

without rearrangement. The barrier to forming cyclobutane cation from the C2 structure is 0.3eV, which is small relative to the excess energy of the system (1.29 eV-1.44 eV). A stabilization of the bridge structure can be obtained via hydrogen migration to the carbon external to the three membered ring, giving isomer 1. The barrier to this hydrogen migration is 0.5 eV, much less than the available energy of the system. Additional chain isomers are also found in this system. Isomers 2 and 3 are probably obtained through a complex mechanism from structure 1 that includes both ring opening and hydrogen migration. The transition state for the hydrogen migration between isomers 2 and 3 is 1.4 eV, which is within the excess energy that the system possesses.

Fragmentations of the above structures are achieved by a loss of either a hydrogen or a methyl radical. The relative intensity of the $C_3H_5^+$ (m/z = 41) peak, is consistent with methyl loss, is higher than the $C_4H_7^+$ (m/z = 55) peak, arising from hydrogen loss, as is evident from the mass spectra at 20 mm (Figure 2). In Figure 7, we present the structures and relative energies of the relevant isomers of $C_3H_5^+$ (red) and $C_4H_7^+$ (purple) which are energetically accessible. The remaining structures can be found in the SI (Figures S6 and S7). The relative energies of the fragmentation products refer to the energy of $C_3H_5^+ + CH_3$ and $C_4H_7^+ + H$.

Isomer 1 of $C_3H_5^+$ is accessible energetically. This isomer can be obtained by the loss of a methyl group from either isomers 1 or 2 of $C_4H_8^+$. For $C_4H_7^+$, structure 1 is obtained by hydrogen loss from the cyclobutane cation and structure 4 can be obtained by hydrogen loss from $C_4H_8^+$ structures 2 and 3. Structure 2 can lead to both products, and we found barriers for hydrogen loss and methyl loss which lie 0.99 eV and 1.17 eV above the C2 isomer respectively. This is energetically well within reach. The corresponding barriers with respect to isomer 2 are 1.89 eV and 2.07 eV respectively. While the barriers are close in energy, the barrier for hydrogen loss is

slightly smaller than the barrier for the methyl loss. As mentioned above, $C_3H_5^+$ can also result from fragmentation of the stable isomer 1, with methyl loss accompanied by a ring opening. The transition state for this reaction is located 1.06 eV above the C2 isomer, which corresponds to a barrier of 2.01 eV.

We attribute the high intensity of the methyl loss peak to the stability and small barrier to form isomer 1 on the $C_4H_8^+$ PES. The small barrier for the hydrogen migration and the stability that results from this transition imply that the system will very rapidly isomerize to isomer 1, from which the only fragmentation route is a methyl loss. It is important to remember however, that the peaks we see are not only results of fragmentation due to dimers, but can also result from fragmentation of larger clusters. In the mass spectrum (Figure 2), one can also observe small peaks m/z = 40 ($C_3H_4^+$) and 42 ($C_3H_6^+$), that could result from fragmentation of the dimer with loss of CH_4 and CH_2, respectively. However, according to our calculations, the $C_3H_6^+$ structures are not energetically accessible from the dimers and must arise from larger clusters.

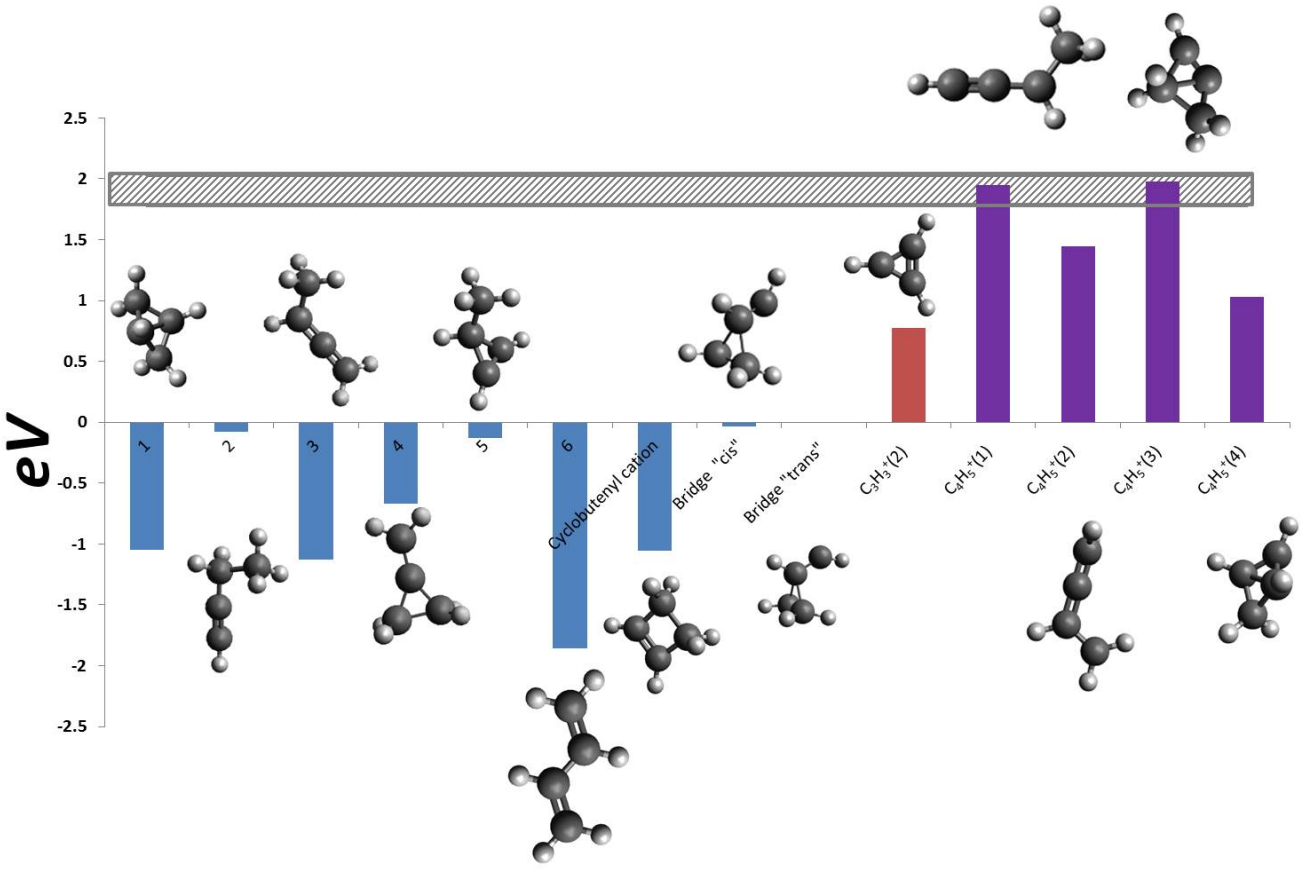

Figure 8. Relative energies of the different $C_4H_6^+$ isomers with respect to the cation optimized bridge structure. In blue are the relative energies of $C_4H_6^+$ isomers. In red is the relative energy of $C_3H_3^+ + CH_3$. In purple is the relative energy of $C_4H_5^+ + H$. Numbers in parentheses refer to isomer labels (see SI). The light gray band from 1.78 eV to 2.03 eV indicates the range of total energies based on vertical ionization of neutral (C_2H_2•C_2H_4).

Figure 8 shows the stable isomers of $C_4H_6^+$ in blue. We found two stable bridge isomers, a cis and a trans isomer, which are very close in energy. As in the previous examples, the most stable isomer that does not include rearrangement of the molecular skeleton is the cyclobutenyl cation, which is lower than the bridge isomer by 1.05 eV. The barrier for crossing between the bridge and the cyclobutenyl cation is less than 0.1 eV and implies a rapid transition to this isomer. The most stable isomers of this system are the chain isomers number 3 and 6. Isomer 6 can be obtained from cyclobutenyl cation through ring opening, for which the barrier is 0.97 eV. The next most stable isomers are four member rings, the cyclobutenyl cation and isomer number 1, which are close in energy. Isomer 1 is not planar and also differs from the bridge structure in the locations of the hydrogens. This isomer can be obtained from the cyclobutenyl cation by a hydrogen migration and ring puckering. The barrier for this rearrangement is 0.96 eV. Three membered rings are also found, with the most stable isomer being isomer number 4. This isomer is obtained by hydrogen migration from the bridge structure, and the barrier to this hydrogen migration is 1.03 eV. We expect that the chain isomers are formed from a more complex mechanism including several steps. The barrier for crossing between the chain isomers, 2 and 3 is 1.71 eV. The system loses its excess internal energy via fragmentation to $C_3H_3^+$ and $C_4H_5^+$. Here again, as is evident from Figure 2, the methyl loss peak is much more intense than the peak for hydrogen loss.

Figure 8 also shows the relevant isomers (the isomers which are energetically accessible) of $C_3H_3^+$ (red) and $C_4H_5^+$ (purple). The energy refers to the energy of $C_3H_3^+ + CH_3$ and $C_4H_5^+ + H$. The rest of the isomers can be found in Figures S8 and S9 in SI. We see that the stable isomer of $C_3H_3^+$ can only result from the loss of a methyl from $C_4H_6^+$ isomer 5. The loss of a methyl radical from either isomer 2 or 3 leads to an energetically inaccessible high energy $C_3H_3^+$ isomer.

$C_4H_5^+$ isomers are higher in energy than $C_3H_3^+$ but are still accessible. Of the $C_4H_5^+$ isomers (Fig. S8), isomer 1 can be obtained by hydrogen loss from $C_4H_6^+$ isomers 2 and 3, while isomer 2 can be obtained by a loss of hydrogen from $C_4H_6^+$ isomer 3 and 6. Isomers 3 and 4 are obtained by loss of hydrogen from the cyclobutenyl cation and isomer 1, respectively. The barrier for a hydrogen loss from isomer 1 ($C_4H_6^+$) to isomer 4 ($C_4H_5^+$) is 2.1 eV. The barrier for hydrogen loss from isomer 3 ($C_4H_6^+$) to isomer 2 ($C_4H_5^+$) is higher, 2.5 eV. Both barriers are within the excess energy of the system: they are 1.04 eV and 1.41 eV above the bridge isomer, respectively.

CONCLUSIONS AND OUTLOOK

We have used VUV photoionization mass spectrometry and theoretical calculations to study mixed reaction products from an acetylene-ethylene expansion. Ionization is carried out at variable distances from the nozzle exit to sample different regimes of the expansion. Intensity distributions of monomers, dimers and reaction products are plotted as a function of ionization distance. The intensity distribution for ethylene and acetylene monomers are low at 2 mm, followed by a maximum at 5 mm and then a gradual decrease. This suggests that association mechanisms starting from monomer cations occur closer to the nozzle due to a higher number density. Other reaction products (m/z = 39, 53 and 65) are observed at all distances with decreasing intensity pattern following the normal density distributions. Theory has been used to study the structures and energetics of neutral and ionized dimers. Furthermore, we have studied the possible isomerization processes and from that obtained mechanistic insight into reaction pathways. For C_4H_4, possible fragmentation channels are hydrogen loss or H_2 loss. Energetically both channels are possible. Fragmentation from $C_4H_8^+$ and $C_4H_6^+$ includes hydrogen-loss and methyl radical loss

channels. While different isomers on the PES are accessible, it is the isomerization rate that dictates fragmentation. For $C_4H_8^+$, rapid isomerization into isomer 1 probably causes a preference for methyl loss. Additional signal for this channel could also arise from larger clusters. The formation of $C_3H_4^+$ and $C_3H_6^+$ cannot occur from a dimer and hence must result from fragmentation of a larger cluster.

The experimental set up essentially has two controls - one can tune the photon energy to precisely ionize a moiety and secondly, change the ionization distance to probe various regions of an expansion. Theory on pure and mixed systems shows several low energy isomers and energetically accessible ones are observed experimentally. A detailed investigation of structure and energetics of larger clusters is currently under way, but our experiment shows that various new products are obtained including cyclic isomers which are the first steps of PAH formation. Product formation are predicted to follow counterintuitive pathways and this combined experimental and theory methodology shows promise in elucidating novel mechanisms in these complex ion-molecule systems. In the present work, we focused on small hydrocarbons, in the future it would be interesting to follow systems which have oxygen embedded in the core. For instance our work on the VUV photoionization dynamics on glycerol and deoxyribose shows that ring opening and closing and strong electrostatic interactions define the reaction and product formation pathways.[41-42]

ASSOCIATED CONTENT

SUPPORTING INFORMATION

The file contains computational structures, Cartesian coordinates and energetics, and photoionization efficiency curves. This material is available free of charge in http://pubs.acs.org.

ACKNOWLEDGEMENTS

This work and the Advanced Light Source are supported by the Director, Office of Science, Office of Basic Energy Sciences, of the U.S. Department of Energy under Contract No. DE-AC02-05CH11231. MHG & TS acknowledge additional support from The National Aeronautics and Space Administration through the NASA Astrobiology Institute under Cooperative Agreement Notice NNH13ZDA017C.

REFERENCES

1. Miller, D., In *Atomic and Molecular Beam Methods*, Scoles, G., Ed. Oxford University Press: 1988; pp 15-23.

2. Pauly, H., *Atom, Molecule and Cluster Beams I* Springer-Verlag, Berlin: 2000; Vol. 1.

3. Duncan, M. A., Invited Review Article: Laser Vaporization Cluster Sources. *Rev. Sci. Instrum.* **2012,** *83*, 041101.

4. Douberly, G. E.; Ricks, A. M.; Ticknor, B. W.; McKee, W. C.; Schleyer, P. v. R.; Duncan, M. A., Infrared Photodissociation Spectroscopy of Protonated Acetylene and Its Clusters. *J. Phys. Chem. A* **2008,** *112*, 1897-1906.

5. Relph, R. A.; Bopp, J. C.; Roscioli, J. R.; Johnson, M. A., Structural Characterization of $(C_2H_2)_{1\text{-}6}^+$ Cluster Ions by Vibrational Predissociation Spectroscopy. *J. Chem. Phys.* **2009,** *131*, 114305-114305.

6. Bandyopadhyay, B.; Kostko, O.; Fang, Y.; Ahmed, M., Probing Methanol Cluster Growth by Vacuum Ultraviolet Ionization. *J. Phys. Chem. A* **2015,** *119*, 4083-4092.

7. Xiao, Y.; Jacob, D. J.; Turquety, S., Atmospheric Acetylene and Its Relationship with CO as an Indicator of Air Mass Age. *J. Geophys. Res.* **2007,** *112*, D12305-19.

8. Courtin, R., Aerosols on the Giant Planets and Titan. *Space Sci Rev* **2005,** *116*, 185-199.

9. Mebel, A. M.; Kislov, V. V.; Kaiser, R. I., Photoinduced Mechanism of Formation and Growth of Polycyclic Aromatic Hydrocarbons in Low-Temperature Environments Via Successive Ethynyl Radical Additions. *J. Am. Chem. Soc.* **2008,** *130*, 13618-13629.

10. Parker, D. S. N.; Zhang, F.; Kim, Y. S.; Kaiser, R. I.; Landera, A.; Kislov, V. V.; Mebel, A. M.; Tielens, A. G. G. M., Low Temperature Formation of Naphthalene and Its Role in the Synthesis of Pahs (Polycyclic Aromatic Hydrocarbons) in the Interstellar Medium. *Proc. Natl. Acad. Sci.* **2012,** *109*, 53-58.

11. Futrell, J. H.; Tiernan, T. O., Ionic Reactions of Unsaturated Compounds. I. Polymerization of Acetylene. *J. Phys. Chem.* **1968,** *72*, 158-164.

12. Tiernan, T. O.; Futrell, J. H., Ionic Reactions in Unsaturated Compounds. Ii. Ethylene. *J. Phys. Chem.* **1968,** *72*, 3080-3093.

13. Ono, Y.; Ng., C. Y., A Study of the Unimolecular Decomposition of the $(C_2H_2)_2^+$ Complex. *J. Chem. Phys.* **1982,** *77*, 2947.

14. Shinohara, H.; Sato, H.; Washida, N., Photoionization Mass Spectroscopic Studies of Ethylene and Acetylene Clusters: Intracluster Excess Energy Dissipation. *J. Phys. Chem.* **1990,** *94*, 6718-6723.

15. Booze, J. A.; Baer, T., The Photoionization and Dissociation Dynamics of Energy-Selected Acetylene Dimers, Trimers, and Tetramers. *J. Chem. Phys.* **1993,** *98*, 186.

16. Coolbaugh, M. T.; Whitney, S. G.; Vaidyanathan, G.; Garvey, J. F., Intracluster Polymerization Reactions within Acetylene and Methylacetylene Clusters Ions. *J. Phys. Chem.* **1992,** *96*, 9139-9144.

17. Kocisek, J.; Lengyel, J.; Farnik, M., Ionization of Large Homogeneous and Heterogeneous Clusters Generated in Acetylene-Ar Expansions: Cluster Ion Polymerization. *J. Chem. Phys.* **2013,** *138*, 124306.

18. Jarrold, M. F.; Bass, L. M.; Kemper, P. R.; van Koppen, P. A. M.; Bowers, M. T., Unimolecular and Bimolecular Reactions in the $C_4H_6^+$ System: Experiment and Theory. *J. Chem. Phys.* **1983,** *78*, 3756-3766.

19. Palm, H.; Alcaraz, C.; Millié, P.; Dutuit, O., State-Selected $C_2H_2^+$+C_2H_4 Reaction: Controlled by Dynamics or Statistics? *Int. J. Mass Spectrom.* **2006,** *249-250*, 31-44.

20. Borden, W. T.; Davidson, E. R.; Feller, D., The Potential Surface for the Cyclobutadiene Radical Cation. *J. Am. Chem. Soc.* **1981,** *103*, 5725-5729.

21. Jungwirth, P.; Carsky, P.; Bally, T., The $C_4H_8^{\bullet+}$ Potential Energy Surface. 1. The Cyclobutane Radical Cation. *J. Am. Chem. Soc.* **1993,** *115*, 5776-5782.

22. Jungwirth, P.; Bally, T., The $C_4H_8^{\bullet+}$ Potential Energy Surface. 2. The $(C_2H_4)_2^{\bullet+}$ Complex Cation and Its Reaction to the Radical Cations of Cyclobutane and 1-Butene. *J. Am. Chem. Soc.* **1993,** *115*, 5783-5789.

23. Hrouda, V.; Roeselová, M.; Bally, T., The $C_4H_4^{\bullet+}$ Potential Energy Surface. 3. The Reaction of Acetylene with Its Radical Cation. *J. Phys. Chem. A* **1997,** *101*, 3925-3935.

24. Hrouda, V.; Bally, T.; Čársky, P.; Jungwirth, P., The $C_4H_4^{\bullet+}$ Potential Energy Surface. 2. The Jahn−Teller Stabilization of Ionized Tetrahedrane and Its Rearrangement to Cyclobutadiene Radical Cation,1. *J. Phys. Chem. A* **1997,** *101*, 3918-3924.

25. Momoh, P. O.; Hamid, A. M.; Abrash, S. A.; Samy El-Shall, M., Structure and Hydration of the $C_4H_4^{\bullet+}$ Ion Formed by Electron Impact Ionization of Acetylene Clusters. *J. Chem. Phys.* **2011,** *134*, 204315.

26. Wiest, O., Structure and [2+2] Cycloreversion of the Cyclobutane Radical Cation. *J. Phys. Chem. A* **1999,** *103*, 7907-7911.

27. Ohta, K.; Nakatsuji, H.; Kubodera, H.; Shida, T., Experimental and Theoretical Study on Cation Radicals of Cyclopropane, Cyclobutane and Cyclopentane. *Chem. Phys.* **1983,** *76*, 271-281.

28. Bera, P. P.; Head-Gordon, M.; Lee, T. J., Association Mechanisms of Unsaturated C2 Hydrocarbons with Their Cations: Acetylene and Ethylene. *Phys. Chem. Chem. Phys.* **2013,** *15*, 2012-2023.

29. Shao, Y.; Gan, Z.; Epifanovsky, E.; Gilbert, A. T. B.; Wormit, M.; Kussmann, J.; Lange, A. W.; Behn, A.; Deng, J.; Feng, X. et. al, Advances in Molecular Quantum Chemistry Contained in the Q-Chem 4 Program Package. *Mol. Phys.* **2015,** *113*, 184-215.

30. Mardirossian, N.; Head-Gordon, M., ωb97x-V: A 10-Parameter, Range-Separated Hybrid, Generalized Gradient Approximation Density Functional with Nonlocal Correlation, Designed by a Survival-of-the-Fittest Strategy. *Phys. Chem. Chem. Phys.* **2014,** *16*, 9904-9924.

31. Behn, A.; Zimmerman, P. M.; Bell, A. T.; Head-Gordon, M., Efficient Exploration of Reaction Paths Via a Freezing String Method. *J. Chem. Phys.* **2011,** *135*, 224108.

32. Chai, J.-D.; Head-Gordon, M., Long-Range Corrected Double-Hybrid Density Functionals. *J. Chem. Phys.* **2009,** *131*, 174105.

33. Kronik, L.; Stein, T.; Refaely-Abramson, S.; Baer, R., Excitation Gaps of Finite-Sized Systems from Optimally Tuned Range-Separated Hybrid Functionals. *J. Chem. Theory Comput.* **2012,** *8*, 1515-1531.

34. Livshits, E.; Granot, R. S.; Baer, R., A Density Functional Theory for Studying Ionization Processes in Water Clusters. *J. Phys. Chem. A* **2011,** *115*, 5735-5744.

35. Lias, S. G., *Ionization Energy Evaluation*. National Institute of Standards and Technology: Gaithersburg MD, 2015; Vol. 69.

36. Kostko, O.; Belau, L.; Wilson, K. R.; Ahmed, M., Vacuum-Ultraviolet (VUV) Photoionization of Small Methanol and Methanol−Water Clusters. *J. Phys. Chem. A* **2008,** *112*, 9555-9562.

37. Belau, L.; Wilson, K. R.; Leone, S. R.; Ahmed, M., Vacuum Ultraviolet (VUV) Photoionization of Small Water Clusters. *J. Phys. Chem. A* **2007,** *111*, 10075-10083.

38. Pendley, R. D.; Ewing, G. E., The Infrared Absorption Spectra of $(HCCH)_2$ and $(DCCD)_2$ *J. Chem. Phys.* **1983,** *78*, 3531-3540.

39. Prichard, D. G.; Nandi, R. N.; Muenter, J. S., Microwave and Infrared Studies of Acetylene Dimer in a T-Shaped Configuration. *J. Chem. Phys.* **1988,** *89*, 115-123.

40. Bryant, G. W.; Eggers, D. F.; Watts, R. O., High-Resolution Infrared Spectroscopy of Acetylene Clusters. *J. Chem. Soc. Faraday Trans.* **1988,** *84*, 1443-1455.

41. Bell, F.; Ruan, Q. N.; Golan, A.; Horn, P. R.; Ahmed, M.; Leone, S. R.; Head-Gordon, M., Dissociative Photoionization of Glycerol and Its Dimer Occurs Predominantly Via a Ternary Hydrogen-Bridged Ion–Molecule Complex. *J. Am. Chem. Soc.* **2013,** *135*, 14229-14239.

42. Ghosh, D.; Golan, A.; Takahashi, L. K.; Krylov, A. I.; Ahmed, M., A VUV Photoionization and Ab Initio Determination of the Ionization Energy of a Gas-Phase Sugar (Deoxyribose). *J. Phys. Chem. Lett.* **2012,** *3*, 97-101.

TOC GRAPHIC